Understanding satellite-derived bathymetry using Sentinel 2 imagery and spatial prediction models

Gema Casal, Paul Harris, Xavier Monteys, John Hedley, Conor Cahalane & Tim McCarthy

Published online: 04 Nov 2019.

Submit your article to this journal

Article views: 632

View related articles

View Crossmark data

Citing articles: 11 View citing articles

Taylor & Francis
Taylor & Francis Group

Check for updates

Understanding satellite-derived bathymetry using Sentinel 2 imagery and spatial prediction models

Gema Casal [ID][a], Paul Harris [ID][b], Xavier Monteys[c], John Hedley[d], Conor Cahalane [ID][e] and Tim McCarthy[a]

[a]National Centre for Geocomputation, Maynooth University, Maynooth, Ireland; [b]Sustainable Agriculture Sciences, Rothamsted Research North Wyke, Devon, UK; [c]Marine & Coastal Unit, Geological Survey Ireland, Dublin, Ireland; [d]Numerical Optics Ltd., Tiverton, UK; [e]Department of Geography, Maynooth University, Maynooth, Ireland

ABSTRACT

Optical satellite data is an efficient and complementary method to hydrographic surveys for deriving bathymetry in shallow coastal waters. Empirical approaches (in particular, the models of Stumpf and Lyzenga) provide a practical methodology to derive bathymetric information from remote sensing. Recent studies, however, have focused on enhancing the performance of such empirical approaches by extending them via spatial information. In this study, the relationship between multibeam depth and Sentinel-2 image bands was analyzed in an optically complex environment using the spatial predictor of kriging with an external drift (KED), where its external drift component was estimated: a) by a ratio of log-transformed bands based on Stumpf's model (KED_S) and b) by a log-linear transform based on Lyzenga's model (KED_L). Through the calibration of KED models, the study objectives were: 1) to better understand the empirical relationship between Sentinel-2 multispectral satellite reflectance and depth, 2) to test the robustness of KED to derive bathymetry in a multitemporal series of Sentinel-2 images and multibeam data, and 3) to compare the performance of KED against the existing *non-spatial* models described by Stumpf *et al.* and Lyzenga. Results showed that KED could improve prediction accuracy with a decrease in RMSE of 89% and 88%, and an increase in R^2 of 27% and 14%, over the Stumpf and Lyzenga models, respectively. The decrease in RMSE provides a worthwhile improvement in accuracy, where results showed effective prediction of depth up to 6 m. However, the presence of higher concentrations of suspended materials, especially river plumes, can reduce this threshold to 4 m. As would be expected, prediction accuracy could be improved through the removal of outliers, which were mainly located in the channel of the river, areas influenced by the river plume, abrupt topography, but also very shallow areas close to the shoreline. These areas have been identified as conflictive zones where satellite-derived bathymetry can be compromised.

1. Introduction

Coastal areas are highly dynamic environments, subject to anthropogenic (e.g. seafloor installations; fishing, habitat modification) and natural pressures (e.g. hazardous storms, erosion, floods) that can be enhanced by climate change effects (Halpern et al. 2008; Lipiec et al. 2018; Gamito et al. 2019). Detailed and frequently updated information about coastal morphology and bathymetry is essential for a variety of commercial, scientific and societal purposes and considered crucial to humankind (Wölf et al. 2019). Bathymetric data can be used for geohazard assessment (Ridente et al. 2014), to monitor seafloor change over time (Chiocci, Cattaneo, and Urgeles 2011; Mielck et al. 2019) and to model change in anticipation of future scenarios (Plecha et al. 2010; Barnard et al. 2019). Wave propagation or bottom currents can produce intensive sediment transport involving important spatial and temporal alterations in the sea bottom topography (Amal et al. 2019; Fan et al. 2019). These intensive and frequent changes in coastal areas demand efficient monitoring methodologies that can produce repetitive updating of bathymetric and seafloor topography information. Precise seafloor information is also required to work toward the goal for protecting at least 10% of the world's oceans by 2020 (Sala et al. 2018) and to support the achievement of SDG 14 - Life below water of the Agenda 2030 for Sustainable Development (Wölf et al. 2019).

Single-or multi-beam echosounders located on board vessels enable high-resolution bathymetric surveys. However, both methods are costly, time-consuming and restricted by coastal morphology, navigation hazards, and protected areas. Their temporal and spatial coverage are dependent on access to the required infrastructure and

---

CONTACT Gema Casal ✉ gema.casal@gmail.com

the associated costs. The use of the airborne LiDAR provides an alternative to extract bathymetry in shallow coastal areas (Chust et al. 2010; Eren et al. 2018), but spatial continuity, hardware, and operational costs, coupled with and logistical requirements reduce the frequency of survey updates. Optical satellite data provide an efficient alternative for bathymetric derivation in shallow coastal waters overcoming financial, temporal and logistical constraints. Interest in this remote sensing solution has increased with the recent availability of Sentinel-2 Multispectral Imager (MSI) that offers improved technical capabilities in comparison with previous optical sensors such as Landsat or SPOT. The MSI instruments on the Sentinel-2A and −2B satellites provide 13 spectral channels ranging from the Visible and the Near-Infrared (VNIR) to the Shortwave Infrared (SWIR), with four bands having a spatial resolution of 10 m. Moreover, the Sentinel-2 mission, being based on a constellation of two identical satellites in the same orbit, offers a nominal revisit time of 5 days, depending on the latitude of the site.

The extraction of bathymetric information from optical remote sensing data can be generally divided into two methodologies: *empirical* and *physics-based* model inversion approaches. Strictly, both approaches are physics-based in that they encompass physical concepts of light transmission through water, such as the assumption that light is attenuated exponentially with depth (Lyzenga 1985). The difference is that empirical methods rely on known bathymetry data points to estimate unknowns through a regression fit, e.g. the rate of spectral light attenuation in the water as a function of depth, whereas model inversion methods more tightly constrain these unknowns and attempt to derive them at each pixel in the image (Brando et al. 2009; Dekker et al. 2011; Hedley et al. 2016). Physics-based approaches can be applied without a-priori known bathymetry points but are more challenging to implement and computationally demanding, hence empirical approaches remain a common and practical method for deriving bathymetry from optical remote sensing data.

Among empirical approaches, the most commonly used are the linear band model (Lyzenga 1985) and the band ratio model (Stumpf, Holderied, and Sinclair 2003). These regression algorithms have been applied to multispectral and hyperspectral sensors with different spatial and spectral resolutions (Lyons, Phinn, and Roelfsema 2011; Bramante, Raju, and Sin 2013; Pacheco et al. 2015; Vahtmäe and Kutser 2016; Traganos et al. 2018). Following these methodologies, recent studies have focused on enhancing the performance of these

empirical models by utilizing spatial information (Curtarelli et al. 2015; Chybiki 2018; Wang et al. 2019). Studies have shown these spatial models to significantly outperform the regular empirical models (Hamylton, Hedley, and Beaman 2015; Su, Liu, and Wu 2015; Kibele and Shears 2016; Cahalane et al. 2019). Among spatial prediction models, kriging is commonly used as it quantifies and exploits the spatial autocorrelation in the data and provides optimal predictions at unsampled locations (Goovaerts 2000). There are also many forms of kriging, where in this study, kriging with an external drift (KED) (see Chiles and Delfiner 1999) was chosen. In KED the spatial autocorrelation effects are accounted for through the residuals of a linear trend fit between the variable of interest (i.e. water depth) and contextual factors (i.e. the reflectance data). In this study, the linear trend (i.e. external drift component) of KED is informed by either a linear combination of log-transformed bands (as in Lyzenga's model) or a ratio of log-transformed bands (as in Stumpf's model) reflecting correlations between reflectance and water depth only. It is expected that the use of KED with either trend/drift component will improve the accuracy of water depth prediction (Su, Liu, and Wu 2015).

In the case of Ireland, much progress in mapping the seafloor has been achieved through the INFOMAR programme, which is currently focused on shallower waters such as bays, with three priority areas located in the east and south of the country. Access to such bays for oceanographic vessels or small boats with acoustic equipment on board is not easy due to associated navigational hazards. In this respect, satellite-derived bathymetry offers an alternative to costly and time-consuming traditional methods such as acoustic surveys. However, the inherent conditions of optically complex waters such as the ones present the Irish coast, have often compromised the results obtained (Coveney and Monteys 2011).

The objectives of this study are: 1) to better understand the empirical relationship between Sentinel-2 multispectral satellite reflectance and depth, 2) to test the robustness of KED to derive bathymetry in a multitemporal series of Sentinel-2 images and multibeam data, and 3) to compare the performance of KED against the existing non-spatial models of Stumpf and Lyzenga. Previous studies have shown the value in using spatial models for bathymetry prediction in Dublin Bay (Monteys et al. 2015). However, the novelty of this study lies on testing the ability of Sentinel-2 products over different time frames, coupled with the removal of outliers to better

inform these models in a practical capacity, rather than the assessment of the models themselves.

2. Materials and methods

2.1 Study area

Dublin Bay is a wide C-shaped inlet located on the east coast of Ireland with an approximately 10 km entrance enclosing an area of about 296 km^2 (Figure 1). This includes the intertidal zone of about 16 km^2 (Brooks et al. 2016) in a relatively flat topography interrupted by tidally controlled related features, such as drainage channels and inlets. The estuary is macro-tidal (Dyer 1973) having a mean tidal range of 2.75 m with an average spring and neap tides of 3.6 m and 1.9 m, respectively (Mansfield 1992). The subtidal benthic area (175 km^2) varies in depth from 25 m to a large inner area less than 5 m (Mansfield 1992). The shores of the bay naturally comprise small areas of rocky and pebbly substrates and very large areas of predominantly fine sand (Brooks et al. 2016). The bay is joined and bisected by the river Liffey in the south and north.

Despite the loss of a significant part of the estuary due to infills, Dublin Bay remains one of the five most important wetlands in the country (Crowe, Boland, and Walsh 2012) with a range of natural habitats that have been designated as part of the European Union Natura 2000 network and recognized by the UNESCO as a Biosphere in 2015 (DCC 2014). High nutrient loads, the deposition of large quantities of organic matter and regular dredging influence the water column conditions (O'Higgins and Wilson 2005). High biomass phytoplankton blooms are frequent in this area which can also reduce optical clarity.

2.2 Multibeam depth data

A number of multibeam transects were acquired on two consecutive years. Survey lines were carried out on the 25/07/2017 and on the 24/03/2018 (Figure 1). Multibeam data were not coincident with satellite overpass; however, their difference in time can be considered acceptable for the aim of this study. The multibeam data have been processed using the hydrographic CARIS HIPS™ suite. Vertical tidal corrections were applied and reduced to LAT (Lowest Astronomical Tide). The resultant depth data meets International Hydrographic Organization (IHO) order 1 standard. Between 0 and 10 m water depth, position uncertainty and the depth error uncertainty were less than 0.5 m and 0.1 m, respectively. The depth data were gridded to 5 m x 5 m using an inverse distance weighted algorithm and subsequently randomly reduced to approximately 2000 data points to optimize computation time for the study prediction models. Only water depths between 0 and 10 m were considered for the subsequent analysis.
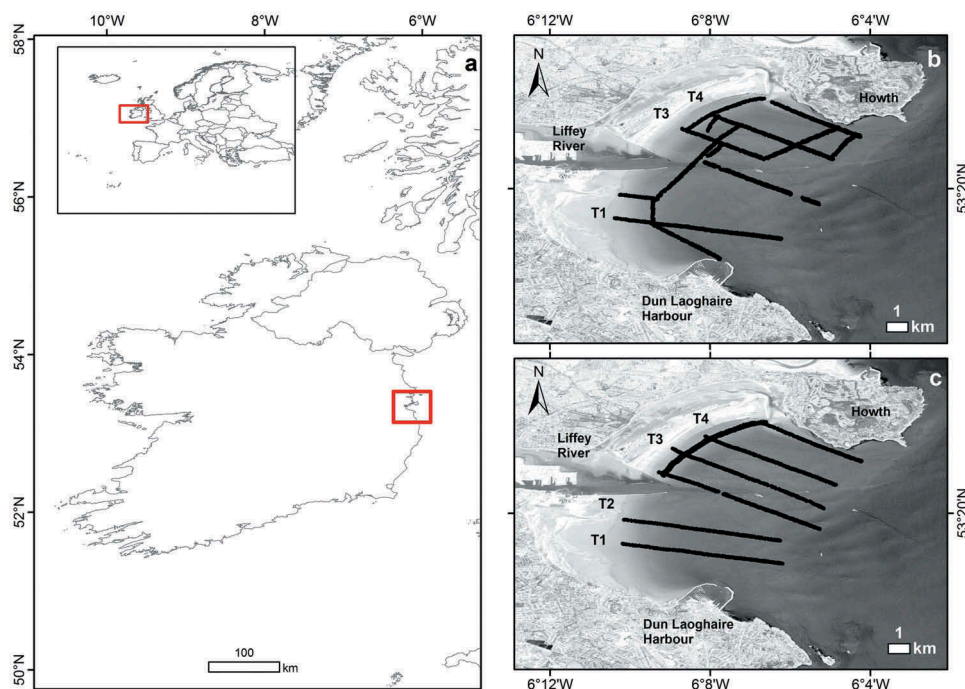

Figure 1. Dublin Bay Study Area (a) location map of study area (b) overlapped the multibeam data registered in 2017 and (c) overlapped the multibeam data registered in 2018. Transects (T1-T4) were individually considered to study the influence of the water column and bottom type in different regions of the bay. T2 is deliberately skipped in figure (b) to keep consistency in terminology between 2017 and 2018 transects.
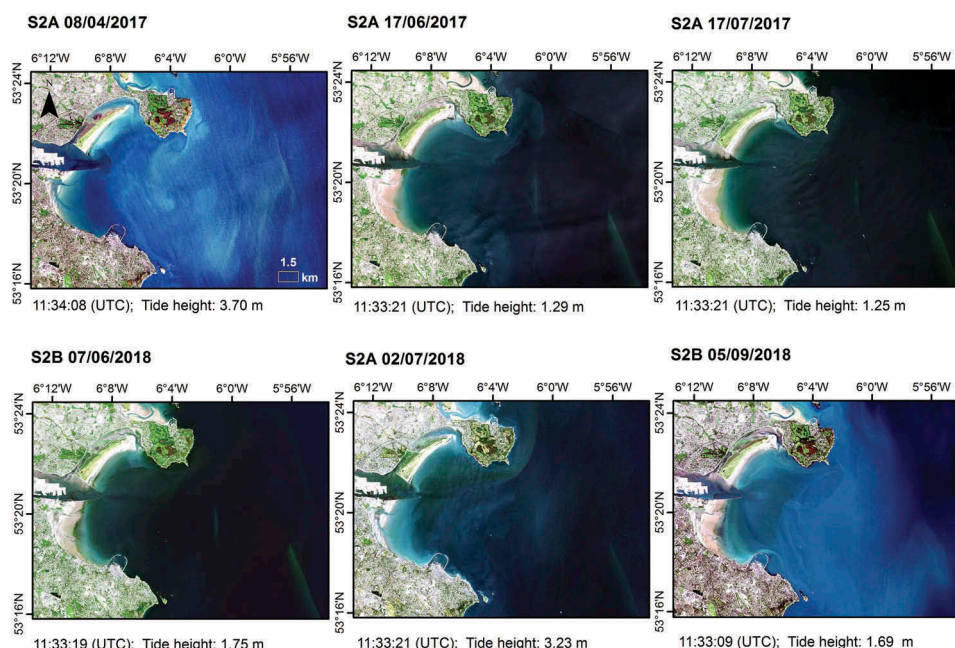
Figure 2. Sentinel-2 images (RGB) included in the study. Acquisition time (UTC) and tide height (m) are showed in each image. Tide height (m) information was provided by the Irish National Tide Gauge Network.

2.3 Remote sensing imagery data

Six Sentinel-2 images were downloaded from the Copernicus Scientific Data Hub website as Level-1C, top-of atmosphere (TOA) reflectance in 100 km x 100 km tiles format and a UTM/WGS84 projection (Figure 2). The images were selected to represent different conditions of the study area: low/high tide, clear/turbid waters and varying degrees of sun glint. Before the application of the study models, all the images were resized to the study area, land was masked out, and atmospheric correction was applied using C2RCC processor (Brockman et al. 2016). C2RCC (Doerffer and Schiller 2007) relies on a large database of simulated water leaving reflectances and related TOA radiances. Neural networks are trained in order to perform the inversion of spectrum for the atmospheric correction, i.e. the determination of the water leaving radiance from the TOA, as well as the retrieval of inherent optical properties of the waterbody (Brockmann et al. 2016). Outputs as water leaving reflectances or remote sensing reflectances can be selected; however, in our case, the latter option was preferred. Previous analysis showed that this processor reduces sun glint effects in the same study area (Casal et al. 2019), for this reason, no additional sun glint correction has been subsequently applied.

Only the 10 m spatial resolution bands B2 (497 nm), B3 (560 nm), and B4 (665 nm) were considered. A preliminary assessment including band B1 was carried out (Casal et al. 2019), but due to its lower spatial resolution (60 m) and its high collinearly with band B2, band B1 was ultimately ruled out of the analyses.

2.4 Geostatistical modeling

The empirical relationships between the multibeam depth data and the Sentinel-2 image bands were statistically analyzed using KED and its drift components. As with any kriging model, KED makes use of the spatial autocorrelation between neighboring observations to predict values at unsampled places together with their uncertainties (Delhomme 1978; Goovaerts 1997; Chiles and Delfiner 1999). KED was chosen for this study as it had previously performed well in the same study area (Monteys et al. 2015), and its use is highly recommended in the physical sciences (Li and Heap 2011). KED model results were assessed and contextualized based on expert knowledge of the study area and previous experience (Monteys et al. 2015).

2.4.1 Exploratory analysis for KED parameterization
To assess the potential of a KED approach, a set of exploratory analyses was carried out. First, a linear correlation analysis between (multibeam) depth and the above-water reflectance (R_w) data was conducted to assess the strength of these relationships. Second, the

residuals from predicting depth using the linear band regression model (Lyzenga 1985) and the residuals from predicting depth using the band ratio regression model (Stumpf, Holderied, and Sinclair 2003) were assessed for spatial autocorrelation through the empirical residual variogram $\gamma_r(h)$:

$$\gamma_r(h) = \frac{\sum_{i=1}^{N_h}[r(s_i + h) - r(s_i)]^2}{2N(h)} \qquad (1)$$

where $r(s_i)$ is the value of the residual from the given regression fit at sampling site s_i, $r(s_i+h)$ is the value of the residual separated from s_i by a distance h (measured in meters), $N(h)$ is the number of pairs of observations separated by the distance or lag (h), and s_i ($i = 1, 2, …, n$) are the n sampled sites.

The variogram is calculated for several lag distances and plotted as a two-dimensional graph with semivariance and distance as the axes. To aid interpretation, a variogram model was fitted to the empirical residual variograms through a weighted least squares (WLS) fit (Cressie 1985). We chose an exponential model form, following that used in Monteys et al. (2015). Variogram parameters: nugget, sill, and range were extracted. The nugget captures small-scale variation; the sill captures structural spatial variation; and the range can be interpreted as the distance beyond which no spatial dependence among the data (in this case, residuals) exists.

The value of the variogram plots is that they graphically illustrate the spatial dependence of the residuals from the Stumpf and Lyzenga models (i.e. the deviations of the Stumpf/Lyzenga model predictions of depth from the actual (multibeam) values of depth). If residual spatial dependence is found to be weak or absent (i.e. a pure nugget variogram), then there would be no value in applying KED, as it would simply default to the respective Stumpf and Lyzenga model fits. A further refinement was also investigated to alleviate the effects of any additional (global) trend in the data (indicated by a linear or parabolic behavior in the variogram). This was done by including the location coordinates to the Lyzenga/Stumpf regression models and re-calculating the regression residuals, accordingly. Observe this residual-based analysis serves for exploratory purposes only. It can have a strong bias due to the ordinary least squares (OLS) estimation of the Lyzenga's and Stumpf's models and also the WLS estimation of the variogram models. This bias is however addressed on estimating the KED model.

2.4.2 Kriging with external drift (KED)

KED is a random function model taking into account, simultaneously, the spatial dependence of the variable of interest (in this case, multibeam data) and its linear relation to one or more explanatory variables (in this case, Sentinel-2 reflectance and also the coordinates). KED consists of a trend (or drift) component and a residual component, where the former is modeled by some linear function (in this study, linear regressions based on the Lyzenga/Stumpf models), while the latter is modeled through ordinary kriging (OK) of the residuals resulting from the linear fit. Depending on how the KED parameters are estimated, there are equivalent models, such as universal kriging and regression kriging (Hengl, Heuvelink, and Rossiter 2007).

In this study, multibeam water depth data can be denoted with their locations as $z(s_1)$, $z(s_2)$, … $z(s_n)$ where we can consider s to be a two-component vector $s = (x, y)$ representing a pixel in the image. For KED, a prediction $\hat{z}(s)$ of depth at any un-sampled location (s) is found by the sum of the regression prediction, $\hat{m}(s)$ and its residual OK prediction, $\hat{r}(s)$:

$$\hat{z}(s) = \hat{m}(s) + \hat{r}(s) \qquad (2)$$

where for this study, $\hat{m}(s)$ is found in two different ways: 1) the prediction of multibeam depth data based on the band ratio regression model (Stumpf, Holderied, and Sinclair 2003) plus coordinates (denoted KED_S):

$$\hat{m}(s)_{\text{KED\_S}} = f\left(\frac{\ln[cR_w(\lambda_{k,s})]}{\ln[cR_w(\lambda_{l,s})]}\right) \qquad (3)$$

where R_w corresponds to the above-water reflectance for the spectral bands k and l after sun glint correction at location s, in our case B2 (470 nm – blue) and B3 (560 nm – green), and c is a fixed constant for ensuring positive log values and a linear response; and 2) the prediction of multibeam depth data based on the linear inversion regression model (Lyzenga 1978, Lyzenga 1985; Lyzenga et al. 2006) plus coordinates (denoted KED_L):

$$\hat{m}(s)_{\text{KED\_L}} = f\left(\sum_{i=1}^{B} a_i \ln[cR_w(\lambda_i)_s]\right) \qquad (4)$$

where B corresponds to the number of the spectral bands considered, a_i ($i = 0,1, … B$) are the model coefficients to be estimated, $R_w(\lambda_j)$ is the above-water reflectance for the spectral band λ_j after sun glint correction. In this study, B2 (470 nm – blue), B3 (560 nm – green), and B4 (665 nm – red) were incorporated to the model.

The residuals $\hat{r}(s)$ in KED were predicted at any un-sampled location (s) using OK:

$$\hat{r}(s) = \sum_{i=1}^{n} w_i(s) \cdot r_K(s_i) \qquad (5)$$

$$\sum_{i=1}^{n} w_i(s) = 1 \qquad (6)$$

where $r_K(s_i)$ represents the residuals from either $\hat{m}(s)_{KED\_S}$ or $\hat{m}(s)_{KED\_L}$; and $w_i(s)$ represents the weights determined by the covariance matrix of $r_K(s_i)$ (i.e. as dictated by the estimated nugget, sill and range parameters of the variogram model).

Observe the residuals $r(s_i)$ defined *for exploration* in Section 2.4.1 and the residuals $r_K(s_i)$ defined *for KED* originate from the same Lyzenga/Stumpf-based regression models, but $r(s_i)$ are biased as they stem from a basic OLS regression estimation, while $r_K(s_i)$ are estimated in a statistically optimal and unbiased fashion. For KED, the regression parameters are now estimated concurrently with the variogram parameters through a generalized least squares (GLS) approach (e.g. Hengl, Heuvelink, and Rossiter 2007), where for this study restricted maximum likelihood (REML) estimation serves this purpose (e.g. Chiles and Delfiner 1999).

KED is applied using a global prediction neighborhood, as opposed to experimentation with local neighborhoods (where any non-stationarity in depth to reflectance relationships would be accounted for, see Monteys et al. 2015). KED can be viewed as statistically optimal, provided the regression and variogram parameters are estimated using REML and provided a global kriging neighborhood is specified. In this form, KED is computationally expensive but is required for best linear-unbiased prediction (BLUP). Accuracy of the KED predictions was measured by the mean prediction error (MPE), the root mean squared prediction error (RMSPE), the relative root mean squared prediction error (RRMSPE) (where the prediction error is the actual depth minus the predicted depth) and the correlation coefficient (r) between the actual and predicted data. For accurate and unbiased prediction, MPE should be zero, RMSPE and RRMSPE should tend to zero and r should be 1. KED is applied using a "leave-one-out" cross-validation procedure to assess the model's ability to predict depth.

Large prediction errors from KED were also used to identify multibeam depth outliers and the same methodological steps of an exploratory analysis for KED and the optimal fit of KED itself were repeated with the outliers removed. Outliers were identified using the Interquartile Range (IQR), which is a simple dispersion measure that can be used to monitor process dispersion in the quality control of the data (Riaz 2013). Methodological steps (exploratory analysis, variograms and KED) were repeated once outliers were identified and removed. This process allowed the identification of conflictive zones for bathymetric derivation as well as zones where this methodology can be considered optimal and applied in a practical context.

3. Results

3.1 Exploratory analysis

The Sentinel-2 image bands for the six images of Figure 2 were log-transformed after atmospheric correction and a constant ($c = 10,000$) was added to ensure positive log values (e.g. Stumpf, Holderied, and Sinclair 2003; Bramante, Raju, and Sin 2013). The multibeam depth data were not transformed to maintain interpretability of the analysis results.

Linear correlation coefficients between the multibeam depth data and the single log-transformed bands and ratios indicated image dependent relationships (Table 1). As described in previous studies (Casal et al. 2019), the strongest image band correlation with depth was observed with the log-transformed Band 3 (560 nm) ($r = -0.96$), indicating that the green band has the highest penetration into the water column. Taking into account all correlations, the weakest correlations were found on 04/08/2017 with r values ranging between -0.08 and 0.12. The strongest r values were found on 07/06/2017 with r values ranging between -0.92 and -0.96 for log-transformed bands. The ratio of log-transformed bands showed $r = 0.86$ for the same date. The correlations between the multibeam depth data and the log-transformed bands tended to be negative, since as the bottom contributes to the reflectance, the reflectance becomes less as water becomes deeper. The correlations between the multibeam depth data and the ratio of log-transformed bands tended to be positive, as this is a function of the relative attenuation in the bands, and therefore depends on which way around the ratio is formed.

Table 1. Linear correlation coefficients between the multibeam depth data and each variable derived from the Sentinel-2 bands, after atmospheric correction, using C2RCC processor, and log transformation have been applied.

Date	Longitude	Latitude	$\ln(R_w (B_2))$	$\ln(R_w (B_3))$	$\ln(R_w (B_4))$	$\ln(R_w (B_2))/\ln(R_w (B_3))$
08/04/2017	0.61	−0.29	0.12	0.1	0.02	−0.08
17/06/2017	0.61	−0.29	−0.79	−0.83	−0.68	0.69
17/07/2017	0.61	−0.29	−0.86	−0.89	−0.79	0.62
07/06/2018	0.66	−0.64	−0.94	−0.96	−0.92	0.86
02/07/2018	0.66	−0.64	−0.76	−0.87	−0.78	0.68
05/09/2018	0.66	−0.64	−0.20	−0.66	−0.81	0.62

It was also useful to identify strong correlations of depth with the coordinates as this can capture broad spatial trends in the data. Since the coast is to the West and depth increases to the East, longitude showed positive correlations with the multibeam depth data for all years in which multibeam data were acquired. However, latitude showed negative correlations with different strengths depending on the image year. In 2018, the correlation of depth with latitude increased in comparison to 2017 due to a change in the spatial distribution/orientation of the sampling transects. Overall the spatial pattern of the multibeam data confirms an expected increment in depth in the East-West direction and the NE orientation of the bay.

Several multibeam depth transects (T1, T2, T3, and T4) (Figure 1) located in homogenous bottom type areas and eliminating conflictive areas were also individually considered using scatterplots (Figures 3 and 4). In this
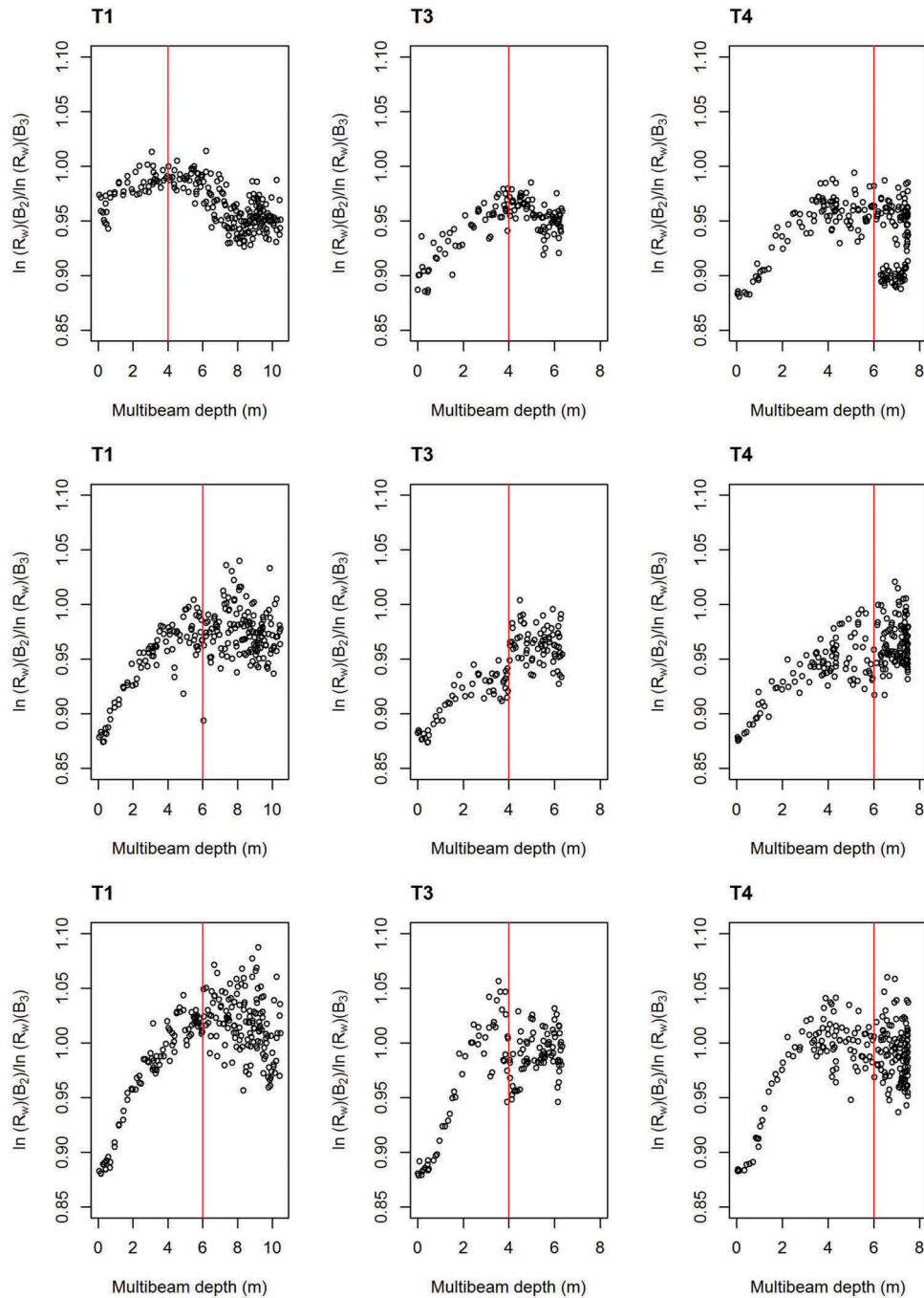

Figure 3. Scatterplots showing the relation between the ratio of atmospherically corrected log-transformed bands (B2 and B3) and multibeam depth for the Sentinel images registered in 2017. T1, T3, and T4 correspond to the multibeam transects carried out in 2017 (shown in Figure 1).
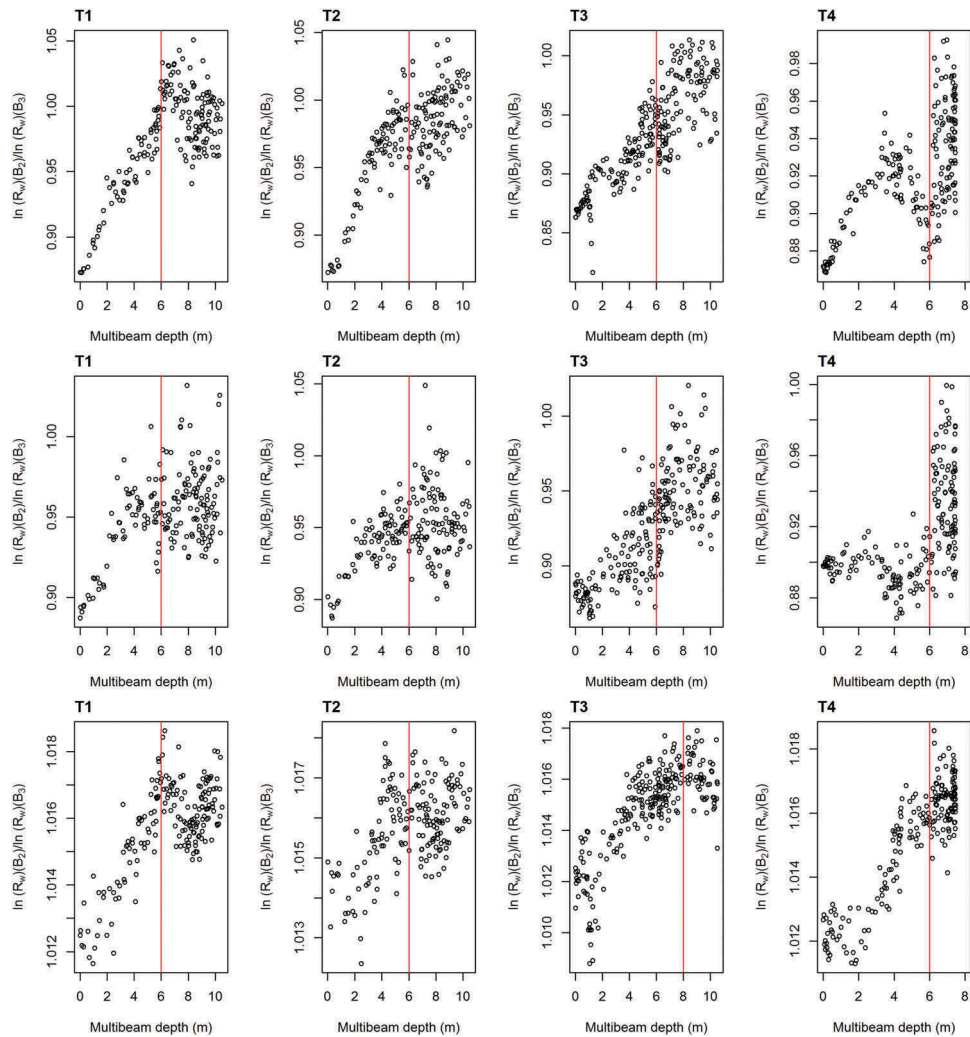
Figure 4. Scatterplots showing the relation between the ratio of atmospherically corrected log-transformed bands (B2 and B3) and multibeam depth for the Sentinel images registered in 2018. T1, T2, T3, and T4 correspond to the multibeam transects carried out in 2018 (shown in Figure 1).

case, the relation between the ratio of log-transformed blue and green bands (ln (R_w (B_2))/ln (R_w (B_3))) against multibeam depth data was plotted. These relations can illustrate the changes in water column conditions and can help to interpret the KED outputs.

For the 2017 images (Figure 3), it can be appreciated how the conditions of turbidity affected the southern part of the bay. This is reflected in the scatterplots correspondent to the image registered on 08/04/2017, the image of highest turbidity registered in 2017. In this case, the increasing linear relationship between reflectance and in situ depth is strong until only 4 m in transects T1 and T3, while this increasing linear relationship is maintained until 6 m in transect T4. The T3 transect is located close to the river channel and thus influenced by water column conditions. The T4 transect is located over a homogenous bottom type area, and thus more likely to ensure a linear relationship at greater depths.

The transect scatterplots of the 2018 images (Figure 4) showed consistence with the ones obtained in 2017. The ratio of log-transformed bands (ln (R_w (B_2))/ln (R_w (B_3))) showed strong linearity with multibeam data until 6 m in transects T1 and T2. The transects sampled in 2018 cover in greater extent the southern part of the Bay confirming that Sentinel-2 images can retrieve depth until 6 m in this part. Due to its proximity to the river channel, the scatterplots of transect T3 are more difficult to interpret. In the case of the image registered on 02/07/2018, a clear plume from the river can be appreciated following north direction (Figure 2). This plume affects transects T2, T3, and T4 and consequently provides weaker relationships in the scatterplots. In the case of the image registered on 05/09/2018, also with a high turbidity, the river plume is more diluted and with different spatial distribution affecting transect T2 the most. In this image (05/09/2018), suspension material is affecting

homogenously the entire study area resulting in a brighter color and consequently, in higher reflectance values. These results suggest that the plume of the river has a greater influence than the suspended material in the level of linearity between the ratio of log-transformed bands and depth.

The exploratory residual variogram analysis in the years 2017 and 2018 consisted of assessing the spatial dependence of the OLS estimated band ratio and linear band regression residuals (noting that both OLS fits were also informed by the coordinates), as well as the influence of outliers. The resultant (outlier removed) residual variograms (12 in total) are given in Figure 5 for residuals from (1) the ratio of log-transformed bands model (i.e. exploration for KED_S parameterization) and (2) the log-transformed linear band model (i.e. exploration for KED_L parameterization).

All residual variograms depicted a clear spatial dependence indicating residuals at nearby locations are more similar than those further apart. As would be expected, the removal of outliers, corresponding with conflictive areas for bathymetry derivation, lowered the residual variogram sill (i.e. the sample variance) over that found with outliers included. The correlation range, i.e. the distance at which the residuals are no longer correlated

with themselves, was approximately 1500 m for many residual variograms, but the variograms associated with the Stumpf's model tended to show a longer range (average 3955 m) than those associated with the Lyzenga's model (average 1060 m). The elimination of outliers in general increased the correlation range. To assess the two different sampling strategies carried out in 2017 and 2018, residual variograms for 2018 were fitted using only the sampling points coincident in location with the ones of 2017. However, little differences were observed. This suggests that, in the context of this study, the sample design was not a major influence on the apparent spatial patterns of association in the residuals from OLS model fits.

3.2 Evaluation of the KED results

Through the statistically unbiased REML parameterization of all KED models (outliers included or not), all image bands were found to be statistically significant predictors of depth (p-value ≤ 0.05) with the exception of B3 (560 nm) and B4 (665 nm) in Lyzenga's model for images registered on the 08/04/2018 and 05/09/2018. The "leave-one-out" prediction accuracy performance for KED_S and KED_L is shown in Table 2, with and
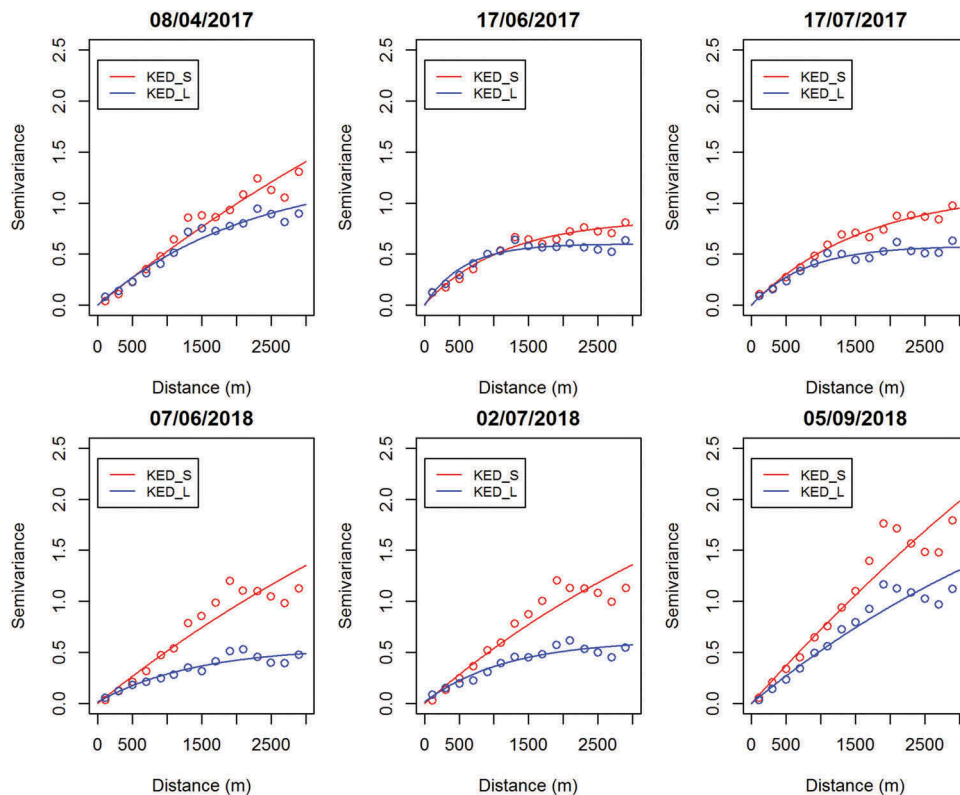

Figure 5. Residual variograms for the ratio of log-transformed bands model, approximation of Stumpf's model (KED_S) and the log-transformed linear band model, approximation of Lyzenga's model (KED_L) – all once the outliers have been removed. Exponential model was used for the WLS fitting (solid lines).

Table 2. Leave-one-out prediction accuracy results between measured and predicted depth for KED_S and KED_L. n = number of points, MPE = mean prediction error and RMSPE = root mean squared prediction error, RRMSPE = relative root mean squared prediction error.

Date	Model	Outliers	n	MPE	RMSPE	Relative RMSPE	Correlation
08/04/2017	KED_S	yes	1651	0.000	0.123	0.045	0.999
08/04/2017	KED_L	yes	1651	0.000	0.136	0.050	0.999
08/04/2017	KED_S	no	1415	0.001	0.103	0.039	0.999
08/04/2017	KED_L	no	1409	0.001	0.106	0.040	0.999
17/06/2017	KED_S	yes	1649	0.000	0.148	0.055	0.999
17/06/2017	KED_L	yes	1649	0.000	0.122	0.046	0.999
17/06/2017	KED_S	no	1407	0.001	0.090	0.034	0.999
17/06/2017	KED_L	no	1507	0.001	0.089	0.033	0.999
17/07/2017	KED_S	yes	1649	0.000	0.168	0.062	0.998
17/07/2017	KED_L	yes	1649	0.000	0.123	0.046	0.999
17/07/2017	KED_S	no	1428	0.001	0.073	0.027	1.000
17/07/2017	KED_L	no	1508	0.000	0.087	0.046	0.999
07/06/2018	KED_S	yes	1710	0.000	0.050	0.014	0.999
07/06/2018	KED_L	yes	1710	0.000	0.078	0.022	0.999
07/06/2018	KED_S	no	1494	0.001	0.041	0.012	1.000
07/06/2018	KED_L	no	1564	0.001	0.052	0.015	1.000
02/07/2018	KED_S	yes	1710	0.000	0.050	0.014	0.999
02/07/2018	KED_L	yes	1710	0.000	0.073	0.020	0.999
02/07/2018	KED_S	no	1501	0.001	0.042	0.012	1.000
02/07/2018	KED_L	no	1512	0.000	0.067	0.019	1.000
05/09/2018	KED_S	yes	1710	0.000	0.050	0.014	0.999
05/09/2018	KED_L	yes	1710	0.000	0.050	0.014	0.999
05/09/2018	KED_S	no	1594	0.000	0.040	0.011	1.000
05/09/2018	KED_L	no	1504	0.001	0.040	0.012	1.000

without outliers. In general, little difference in prediction accuracy was found with KED_S and KED_L when outliers were accounted for and the results tended to be image dependent. As would be expected, prediction accuracy improved through the removal of outliers, where KED_S tended to provide more accurate predictions than KED_L. Thus, KED_L was more susceptible to outliers, and for this reason, we could consider KED_S as the best predictor for water depth in Dublin Bay.

Scatterplots of actual versus KED predictions for KED_S and KED_L showed the largest prediction errors in shallow waters (<1 m) and areas deeper than 6 m. The largest prediction errors occur around the deep channel and in areas close to the Howth peninsula and can be a result of both over- and under-prediction. Both areas present a rough topography, with rock outcrops in the case of the Howth area, and high backscatter in the multibeam data (Monteys et al. 2015). The influence of variations in water column optical properties on the satellite-derived depth has been evaluated through the scatterplots of KED prediction errors versus KED predicted depth, once outliers were removed (Figure 6). The results of both KED models were again coincident indicating a reduction in prediction accuracy at 6 m depths and below in all the images (noting that for some transects, this threshold is likely to be 4 m, from the scatterplots in Figures 3 and 4). KED prediction accuracy at shallow depths under 1 m was also found to vary between models and data sets.

Identified outliers were mapped as a simple way to visually examine the spatial distribution of conflictive zones for bathymetry derivation in Dublin Bay and to get a handle on their causes (Figure 7). Outliers identified in both models, KED_S and KED_L, were located in very specific areas that were coincident in both cases. These areas mainly corresponded to the channel of the Liffey River (high turbidity), an area off the Howth peninsula, coincident with abrupt topography and rock outcrops, and very shallow areas close to the shoreline. The transects carried out in 2017 also showed a conflictive zone close to the piers of Dun Laoghaire Harbor. However, this issue could not be evaluated in the images of 2018 due to the lack of transects in this area.

Finally, for context, it is important to compare KED results with results from their respective trend or drift component fits – i.e. the OLS regression models developed by Stumpf and Lyzenga. Here their extensions to a spatial form in KED_S and KED_L performed more accurately with a decrease in RMSE of 89% and 88%, and an increase in R^2 of 27% and 14%, over their Stumpf's and Lyzenga's models (Casal et al. 2019), respectively. This improvement in performance is shown in Figure 8, where KED clearly reduces predictions error. In the case of the OLS models, the highest under-predicted and over-predicted depths were limited to specific areas. For example, the OLS models tended to under-predict depth in shallow areas while in deep areas tended to over-predict. However, the highest prediction errors tended to be located in the same areas, for all models applied.

Observe that we have not presented KED prediction maps of the whole study area, as their quality can, in
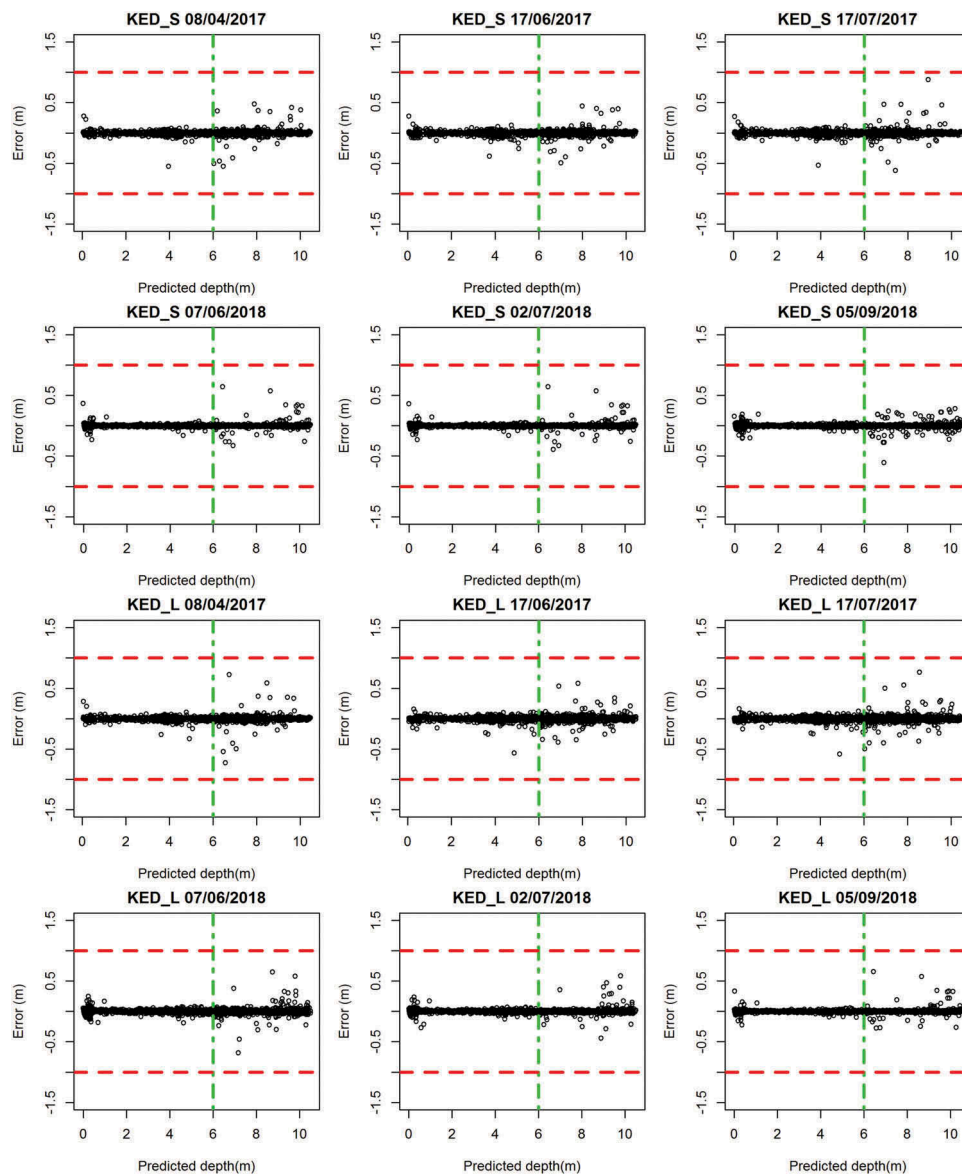
Figure 6. Scatterplots for satellite predicted depth using KED_S and KED_L and the corresponding KED prediction errors after outliers have been removed. Prediction errors are represented in meters (m). The green line marks the depth where KED prediction errors increase and scatter the most. The red lines mark the KED prediction errors above +1 and below −1.

part, be dependent on the spatial configuration of in-situ data (given in Figure 1) which are very linear in nature. This may give rise to spurious spatial artifacts on the KED surface. It is recommended that future ground-reference in-situ sampling should ensure a better spatial representation of the entire bay.

4. Discussion

Through this study's exploratory analysis, the Sentinel-2 band that exhibited the highest correlation with in situ depth was Band 3 (560 nm) corresponding to the green part of the electromagnetic spectrum. This result is consistent with previous studies carried out in the same study area (Casal et al. 2019) and with other studies carried out in turbid waters (Vahtmäe and Kutser 2016). While in clear waters the blue band should be selected for bathymetry retrieval due to its higher penetration into the water column, in waters containing dissolved organic matter (CDOM) the optimal bands shift to longer wavelengths such as green and yellow spectral regions. The correlation between reflectance and in situ depth was also image dependent indicating that the local water column conditions at the time of the image acquisition can affect the relation between reflectance and depth.
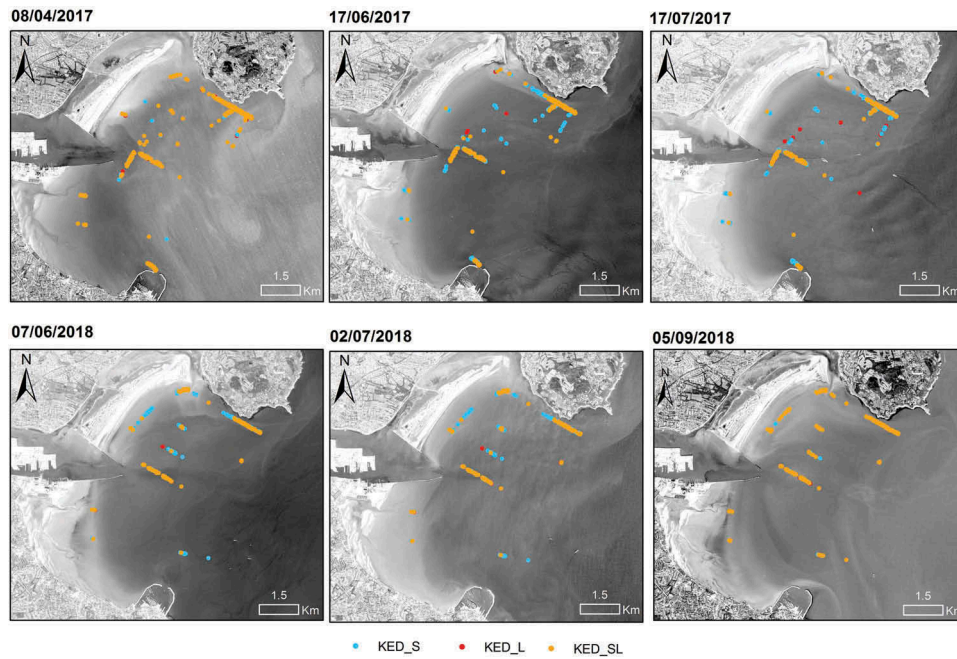
Figure 7. Outliers resultant from the KED_L (red) and KED_S (blue) calibration. Outliers coincident in both calibrations, KED_SL, are shown in yellow. Only sampling points coincident in both campaigns 2017 and 2018 have been considered.
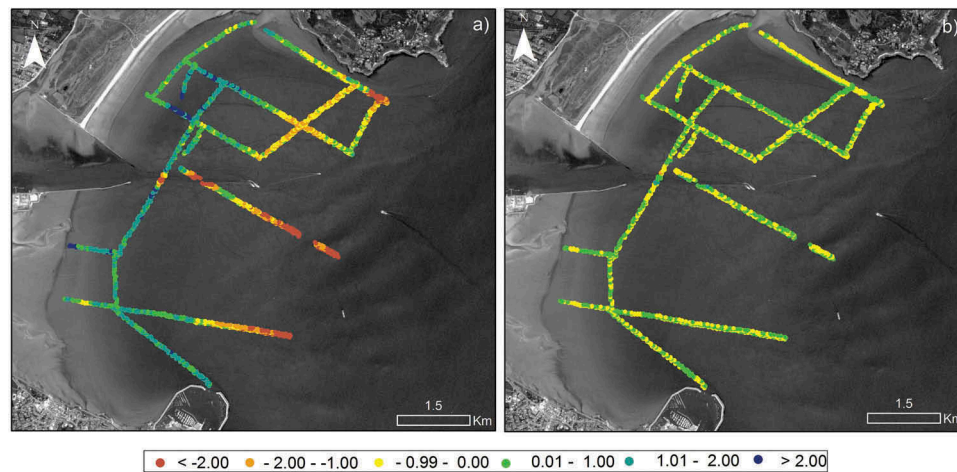

Figure 8. Example of mapped prediction errors (in meters) for the Sentinel-2 image registered on 17/07/2017. a) Stumpf's OLS regression method (Casal et al. 2019). b) KED_S.

Through a spatially explicit analysis of the data, a greater understanding of the relationship between depth and Sentinel-2 bands is possible. Results showed consistence between images where models seemed to be less sensitive to water quality conditions. Spatial models in KED_S and KED_L performed better in comparison with their non-spatial counterparts with smaller prediction errors (see Casal et al. 2019), which is viewed as a significant improvement in prediction accuracy.

This improvement in prediction accuracy by the spatial prediction models was also found in comparison with other studies that used empirical algorithms and

Sentinel-2 data. For example, Traganos et al. (2018) predicted bathymetry (0–12 m) from Sentinel-2 data using Lygenza's and Stumpf's models, including blue and green bands, in the coastal areas of the Aegean Sea. For Lyzenga's model, these authors reported an R^2 of 0.69, while for Stumpf's model they reported an R^2 of 0.5, being these values lower than the ones obtained here using spatial prediction models. In the study of Traganos et al. (2018) the highest R^2 value ($R^2 = 0.9$) was obtained for Lyzenga's model after applying optimization steps such as a 3×3 smoothed filter and a normalized median Sentinel-2 composite. Studies assessing the application

of spatial prediction models to Sentinel-2 data are still scarce and only a few examples have been found for comparison with our study. We could mention the study carried out by Chybicki in 2018 (Chybiki 2018) that developed a novel spatial prediction method (spatial prediction three-dimensional geographically weighted inverse regression) to derive bathymetry in the Baltic Sea and reported correlation coefficients (*r*) of actual versus predicted between 0.92 and 0.96.

Spatial studies using other satellite products include that of Hamylton, Hedley, and Beaman (2015) for two sites on the Great Barrier Reef using WorldView-2 images, where models based on Stumpf's (using blue and green bands) and optimization methods such as the adaptive look-up table (ALUT) model inversion method (Hedley, Roelfsema, and Phinn 2009; Hedley et al. 2012) were assessed. An extension to a spatial error model was constructed which significantly improved model performance, reporting R^2 values of 0.95. Su, Liu, and Wu (2015) compared Lyzenga's model with its extension to regression kriging (which is mathematically equivalent to KED, see Hengl, Heuvelink, and Rossiter 2007) on the coast of Hawaii using IKONOS multispectral images. Here, the regression kriging model (R^2 = 0.95) only increased R^2 by 2% in comparison with the Lyzenga's model (R^2 = 0.93). This small gain could be in part explained due to the temporal difference between the LiDAR in situ depth (2000) and the IKONOS image (2005) used, and also the use of different datasets for model calibration and validation. Our findings and comparisons demonstrate that the combination of Sentinel-2 data and KED is a powerful and consistent method to derive accurate bathymetry in coastal shallow waters.

A key outcome of our study was the identification of areas where the derivation of bathymetry using satellite imagery can be compromised. Outliers identified for KED_S and KED_L were coincident in location for all analyzed images. These areas corresponded to the channel of the Liffey River, an area off the Howth Peninsula and very shallow areas close to the shoreline. These areas were similarly identified in Monteys et al. (2015) using spatial models but a single RapidEye image. Results indicate that the discharges of the river and the abrupt topography of the channel have an important influence on the relationship between reflectance and in situ depth. This influence is critical even when turbid events do not occur. The northern part of the bay, close to Howth Peninsula, is affected by the river plume due to the hydrodynamic conditions of the bay (Dublin Port Company 2017), where this area also corresponds with an abrupt topography and rock outcrops. Outliers were also detected close to the shoreline indicating the influence of the bottom

type in satellite-derived depth. Both KED_S and KED_L performed similarly across all study images, but when outliers were removed, KED_S provided better fit, which could be explained by the Stumpf's model premises. Stumpf's algorithm assumes that changes in bottom reflectance affect the band ratio insignificantly compared to changes in depth. A change in bottom albedo affects both bands similarly, while changes in depth have a more pronounced effect on the band with greater attenuation. This algorithm has also been shown to better account for turbidity (Stumpf, Holderied, and Sinclair 2003).

Study results showed that turbidity, especially river plumes, bottom type, and topography exert an influence on the accuracy and precision of satellite-derived bathymetry and these factors need to be considered to obtain accurate bathymetric maps. Wave environment and natural spring-neap-spring cycles have been reported to be the main drivers of turbidity events in Dublin Bay (Dublin Port Company 2017). In our case, three out of the six images presented different degrees of turbidity conditions. The highest intertidal range (3 m) found in the Sentinel-2 image registered on the 02/07/2018 could be a possible explanation about the more located turbidity close to the coast. In the images registered on the 08/04/2017 and on the 05/09/2018, practically the entire bay is affected by turbidity that could be a consequence of suspension material produced by high waves of Storms Doris (late February 2017) and Ernesto (mid-August 2018). In our case, sample design proved to have little influence on model performance, as the transect orientations and distributions were similar across data sets. Here, the availability of in situ data covering all bottom types and water quality conditions is likely to improve prediction accuracy (Monteys et al. 2015; Casal et al. 2019).

This influence of bottom type and water transparency has been reported by other studies (e.g. Lafon et al. 2002; Vahtmäe and Kuster 2016; Caballero and Stumpf 2019) where water turbidity has been stated as the most significant factor in influencing satellite-derived bathymetry precision (Dekker et al. 2011). Suspended particulate matter, a main contributor of turbidity, backscatters light from the water column, typically producing an under-prediction of depth. Additionally, waters with differing degrees of turbidity can scatter the incoming radiation differently, introducing further complexity in highly dynamic coastal regions (Caballero and Stumpf 2019). For this reason, the availability of methods that can make a first assessment about the relation between reflectance and real depth, taking into account local conditions, as with the robust spatial models of this study, is fundamental.

This study demonstrated that in Dublin Bay, where homogenous bottom and no turbidity events such as

suspension material or river plumes exist, bathymetry can be reliably derived up to a depth of 6 m using Sentinel-2 data. This result is coincident with previous studies using non-spatial empirical methods and Sentinel-2 data in the same study area (Casal et al. 2019), confirming 6 m as the critical depth for "optimal" satellite-derived bathymetry. In other studies, carried out in Dublin Bay, bathymetry was reported to be satisfactorily retrieved up until 12 m using spatial empirical methods and a RapidEye image (Monteys et al. 2015). These differences are likely due to the different distribution of the in-situ depth sampling points that in the case of the RapidEye analysis were homogeneously distributed over the whole study area. Conversely, other studies carried out in turbid waters such as the Guadiana estuary (Spain) (Sánchez-Carnero et al. 2014) or South Florida (USA) (Caballero and Stumpf 2019) reported a similar depth limit of 6 m, using SPOT images and Sentinel-2 with a 10 m spatial resolution. This suggests a limit of around 6 m could be a conservative approximation for turbid waters in general.

5. Conclusions

In this study, the empirical relationship between multibeam depth data and Sentinel-2 was analyzed using the spatial prediction method of kriging with an external drift (KED) for Dublin Bay, Ireland, across multiple years. Results showed improved prediction accuracies in satellite-derived bathymetry in comparison with simpler non-spatial constructions, decreasing RMSE by more than 80%. Results suggest that Sentinel-2 data could be used to effectively capture depth in Dublin Bay until 6 m. However, the presence of higher concentration of suspended materials, especially river plumes, can influence these results reducing this threshold to 4 m. The combined use of Sentinel-2 data (10 m bands) and KED is considered a powerful and robust tool to derive accurate bathymetry in coastal shallow waters and to define local conflictive areas for this purpose.

Highligths

- Spatial prediction models can accurately derive satellite depth until 6 m in Dublin Bay
- KED improved depth prediction accuracy in comparison with simpler non-spatial models
- Turbidity, abrupt topography, and bottom signal are the main factors influencing satellite-derived bathymetry

Acknowledgements

Disclosure statement

Funding

ORCID

Gema Casal http://orcid.org/0000-0002-3346-8035
Paul Harris http://orcid.org/0000-0003-0259-4079
Conor Cahalane http://orcid.org/0000-0003-1657-5688

References

Amal, R., E. W. J. Bergsma, P. Maisongrande, and L. P. Melo de Almeida. 2019. "Wave-derived Coastal Bathymetry from Satellite Video Imagery: A Showcase with Pleiades Persistent Mode." *Remote Sensing of Environment* 231: 111263. doi:10.1016/j.rse.2019.111263.

Barnard, P. L., L. H. Erikson, A. C. Foxgrover, J. A. Finzi Hart, P. Limber, A. C. O'Neill, M. van Ormondt, et al. 2019. "Dynamic Flood Modelling Essential to Assess the Coastal Impacts of Climate Change." *Nature* 9: 4309.

Bockmann, C., R. Doerffer, M. Peters, K. Stelzer, S. Embacher, and A. Ruescas. 2016. "Evolution of the C2RCC Neural Network for Sentinel 2 and 3 for the Retrieval of Ocean Colour Products in Normal and Extreme Optically Complex Waters". In *Proceedings of the Living Planet Symposium 2016*, Prague, Czech Republic, 9-13 May 2016.

Bramante, J. F., D. K. Raju, and T. M. Sin. 2013. "Multispectral Derivation of Bathymetry in Singapore's Shallow, Turbid Waters." *International Journal of Remote Sensing* 34 (6): 2070–2088. doi:10.1080/01431161.2012.734934.

Brando, V., J. M. Anstee, M. Wettle, A. G. Dekker, S. R. Phinn, and C. Roelsfsema. 2009. "A Physics Based Retrieval and Quality Assessment of Bathymetry from Suboptimal Hyperspectral Data." *Remote Sensing of Environment* 113 (4): 755–770. doi:10.1016/j.rse.2008.12.003.

Brooks, P. R., R. Nairn, M. Harris, D. Jeffrey, and T. P. Crowe. 2016. "Dublin Port and Dublin Bay: Reconnecting with Nature and People." *Regional Studies in Marine Science* 8: 234–251. doi:10.1016/j.rsma.2016.03.007.

Caballero, I., and R. Stumpf. 2019. "Retrieval of Nearshore Bathymetry from Sentinel-2A and 2B Satellites in South Florida Coastal Waters." *Estuarine, Coastal and Shelf Science* 226: 106277. doi:10.1016/j.ecss.2019.106277.

Cahalane, C., A. Magee, X. Monteys, G. Casal, J. Hanafin, and P. Harris. 2019. "A Comparison of Landsat 8, RapidEye and Pleiades Products for Improving Empirical Predictions of Satellite-derived Bathymetry." *Remote Sensing of Environment* 233: 111414. doi:10.1016/j.rse.2019.111414.

Casal, G., X. Monteys, J. Hedley, P. Harris, C. Cahalane, and T. McCarthy. 2019. "Assessment of Empirical Algorithms for Bathymetry Extraction Using Sentinel-2 Data." *International Journal of Remote Sensing* 40 (8): 2855–2879. doi:10.1080/01431161.2018.1533660.

Chiles, J. P., and P. Delfiner. 1999. *Geostatistics-Modelling Spatial Uncertainty*. New York, NY: Wiley.

Chiocci, F. L., A. Cattaneo, and R. Urgeles. 2011. "Seafloor Mapping for Geohazard Assessment: State of the Art." *Marine Geophysical Research* 32 (1–2): 1–11. doi:10.1007/s11001-011-9139-8.

Chust, G., M. Grance, I. Galparsoro, A. Uriarte, and A. Borja. 2010. ""Capabilities of the Bathymetric Hawk Eye LiDAR for Coastal Habitat Mapping: A Case of Study within A Basque Estuary." *Estuarine, Coastal and Shelf Science* 89 (3): 200–213. doi:10.1016/j.ecss.2010.07.002.

Chybiki, A. 2018. "Three-Dimensional Geographically Weighted Inverse Regression (3GWR) Model for Satellite Derived Bathymetry Using Sentinel-2 Observations." *Marine Geodesy* 41 (1): 1–23. doi:10.1080/01490419.2017.1373173.

Coveney, S., and X. Monteys. 2011. "Integration Potential of INFOMAR Airborne LIDAR Bathymetry with External Onshore LIDAR Data Sets." *Journal of Coastal Research* 62: 19–29. doi:10.2112/SI_62_3.

Cressie, N. 1985. "Fitting Variogram Models by Weighted Least Squares." *Mathematical Geology* 17 (5): 563–587. doi:10.1007/BF01032109.

Crowe, O., H. Boland, and A. Walsh. 2012. "Irish Wetland Bird Survey: Results of Monitoring Ireland in 2010/11." *Irish Birds* 9: 397–410.

Curtarelli, M., J. Leão, I. Ogashawara, J. Lorenzzetti, and J. Stech. 2015. "Assessment of Spatial Interpolation Methods to Map the Bathymetry of an Amazonian Hydroelectric Reservoir to Aid in Decision Making for Water Management." *ISPRS Journal of Photogrammetry and Remote Sensing* 4: 220–235.

Dekker, A. G., S. R. Phinn, J. Anstee, P. Bissett, V. E. Brando, B. Casey, P. Fearns, et al. 2011. "Intercomparison of Shallow Water Bathymetry, Hydro-optics, and Benthos Mapping Techniques in Australian and Caribbean Coastal Environment." *Limnology and Oceanography: Methods* 9: 396–425.

Delhomme, J. P. 1978. "Kriging in the Hydrosciences." *Advances in Water Resources* 1: 251–266. doi:10.1016/0309-1708(78)90039-8.

Doerffer, R., and H. Schiller. 2007. "The MERIS Case 2 Water Algorithm." *International Journal of Remote Sensing* 28 (3): 517–535. doi:10.1080/01431160600821127.

Dublin City Council (DCC). 2014. In *North Bull Island UNESCO Biosphere-Periodic Review*, edited by M. Harris. Dublin City Council Dublin. Accessed 30 October 2019 www.dublinbaybiosphere.ie

Dublin Port Company. 2017. *Annual Environmental Report 2017*. Dumpling at Sea Permit S0024-01. Belfast, Ireland. 127

Dyer, K. R. 1973. *Estuaries: A Physical Introduction*. Chichester: Wiley.

Eren, F., S. Pe'eri, Y. Rzhanov, and L. Ward. 2018. "Bottom Characterization by Using Airborne Lidar Bathymetry (ALB) Waveform Features Obtained from Bottom Return Residual Analysis." *Remote Sensing of Environment* 203 (1): 260–274. doi:10.1016/j.rse.2017.12.035.

Fan, R., H. Wei, L. Zhao, C. Jiang, and H. Nie. 2019. "Identify the Impacts of Waves and Tides to Coastal Suspended Sediment Concentration Based on High-Frequency Acoustic Observations." *Marie Geology* 408: 154–164. doi:10.1016/j.margeo.2018.12.005.

Gamito, R., C. Pita, C. Teixeira, M. J. Costa, and H. N. Cabral. 2019. "Trends in Landings and Vulnerability to Climate Change in Different Fleet Components in the Portuguese Coast." *Fisheries Research* 181: 93–101. doi:10.1016/j.fishres.2016.04.008.

Goovaerts, P. 1997. *Geostatistics for Natural Resources Evaluation*. New York, NY: Oxford University Press.

Goovaerts, P. 2000. "Geostatistical Approaches for Incorporating Elevation into the Spatial Interpolation of Rainfall." *Journal of Hydrology* 228 (1–2): 113–129. doi:10.1016/S0022-1694(00)00144-X.

Halpern, B. S. S., K. A. Walbridge, C. V. Selkoe, K. F. Micheli, C. D'Agrosa, J. F. Bruno, K. S. Casey, et al. 2008. "A Global Map of Human Impact on Marine Ecosystems." *Science* 319: 948–952. doi:10.1126/science.1149345.

Hamylton, S. M., J. Hedley, and R. J. Beaman. 2015. "Derivation of High-Resolution Bathymetry from Multispectral Satellite Imagery: A Comparison of Empirical and Optimisation Methods through Geographical Error Analysis." *Remote Sensing* 7: 16257–16273. doi:10.3390/rs71215829.

Hedley, J., C. Roelfsema, B. Koetz, and S. Phinn. 2012. "Capability of the Sentinel 2 Mission for Tropical Coral Reef Mapping and Coral Bleaching Detection." *Remote Sensing of Environment* 120: 145–155. doi:10.1016/j.rse.2011.06.028.

Hedley, J., C. Roelfsema, and S. R. Phinn. 2009. "Efficient Radiative Transfer Model Inversion for Remote Sensing Applications." *Remote Sensing of Environment* 113: 2527–2532. doi:10.1016/j.rse.2009.07.008.

Hedley, J., B. Russell, K. Randolph, and H. Dierssen. 2016. "A Physics-Based Method for the Remote Sensing of Seagrasses." *Remote Sensing of Environment* 174: 134–147. doi:10.1016/j.rse.2015.12.001.

Hengl, T., G. B. M. Heuvelink, and D. G. Rossiter. 2007. "About Regression-Kriging: From Equation to Case Studies." *Computers and Geosciences* 33: 1301–1315. doi:10.1016/j.cageo.2007.05.001.

Kibele, J., and N. T. Shears. 2016. "Nonparametric Empirical Depth Regression for Bathymetric Mapping in Coastal Water." *IEEE Journal of Selected Topics in Applied Earth Observations and Remote Sensing* 9 (11): 5130–5138. doi:10.1109/JSTARS.2016.2598152.

Lafon, V., J. M. Froidefond, F. Lahet, and P. Castaing. 2002. "SPOT Shallow Water Bathymetry of a Moderately Turbid Tidal Inlet Based on Field Measurements." *Remote Sensing of Environment* 81: 136–148. doi:10.1016/S0034-4257(01)00340-6.

Li, J., and A. D. Heap. 2011. "A Review of Comparative Studies of Spatial Interpolation Methods in Environmental Sciences: Performance and Impact Factors." *Ecological Informatics* 6 (3–4): 228–241. doi:10.1016/j.ecoinf.2010.12.003.

Lipiec, E., P. Ruggiero, A. Mills, K. A. Serafin, J. Bolte, P. Corcoran, J. Stevenson, C. Zanocco, and D. Lach. 2018. "Mapping Out Climate Change: Assessing How Coastal Communities Adapt Using Alternative Future Scenarios." *Journal of Coastal Research* 34 (5): 1196–1208. doi:10.2112/JCOASTRES-D-17-00115.1.

Lyons, M., S. Phinn, and C. Roelfsema. 2011. "Integrating Quickbird Multispectral Satellite and Field Data: Mapping Bathymetry, Seagrass Cover, Seagrass Species and Change in Moreton Bay, Australia in 2004 and 2007." *Remote Sensing* 3 (1): 42–64. doi:10.3390/rs3010042.

Lyzenga, D. R. 1985. "Shallow-water Bathymetry Using Combined LiDAR and Passive Multispectral Scanner Data." *International Journal of Remote Sensing* 6: 115–125. doi:10.1080/01431168508948428.

Lyzenga, D. R., N.P. Malinas, and F.J. Tanis 2006. "Multispectral bathymetry using a simple physically based algorithm." *IEE Transactions on Geoscience and Remote Sensing* 44: 2251–2259. doi:10.1109/TGRS.2006.872909.

Mansfield, M., 1992. *Dublin Bay Water Quality Management Plan: Field Studies of Currents and Dispersion*. Technical Report 3. Ireland: Environmental Research Unit.

Mielck, F., H. C. Hass, R. Michaelis, L. Sander, S. K. H. Papenmeier, and Wiltshire. 2019. "Morphological Changes Due to Marine Aggregate Extraction for Beach Nourishment in the German Bight (SE North sea)." *Geo-Marine Letters* 39: 47–58. doi:10.1007/s00367-018-0556-4.

Monteys, X., P. Harris, S. Caloca, and C. Cahalane. 2015. "Spatial Prediction of Coastal Bathymetry Based on Multispectral Imagery and Multibeam Data." *Remote Sensing* 7: 13782–13806. doi:10.3390/rs71013782.

O'Higgins, T. G., ., and J. G. Wilson. 2005. "Impact of the River Liffey Discharge on Nutrient and Chlorophyll Concentrations in the Liffey Estuary and Dublin Bay (Irish sea)." *Estuarine, Coastal and Shelf Science* 64: 323–334. doi:10.1016/j.ecss.2005.02.025.

Pacheco, A., J. Horta, C. Loureiro, and O. Ferreira. 2015. "Retrieval of Nearshore Bathymetry from Landsat 8 Images: A Tool for Coastal Monitoring." *Remote Sensing of Environment* 159: 102–116. doi:10.1016/j.rse.2014.12.004.

Plecha, A. P. A., S. N. Vaz, X. Bertin, A. Oliveira, A. B. Fortunato, and J. M. Dias. 2010. "Sensitivity Analysis of a Morphodynamic Modelling System Applied to a Coastal Lagoon Inlet." *Ocean Dynamics* 60 (2): 275–284. doi:10.1007/s10236-010-0267-5.

Riaz, M. 2013. "On Enhanced Interquartile Range Charting for Process Dispersion." *Quality and Reliability Engineering International* 31 (3): 389–398. doi:10.1002/qre.1598.

Ridente, D., E. Martonelli, A. Bosman, and F. L. Chiocci. 2014. "High-Resolution Morpho-Bathymetric Imaging of the Messina Strait (Southern italy). New Insights on the 1908 Earthquake and Tsunami." *Geomorphology* 208: 149–159. doi:10.1016/j.geomorph.2013.11.021.

Sala, E., J. Lubchenco, K. Grorud-Colvert, C. Novelli, C. Roberts, and U. R. Sumaila. 2018. "Assessing Real Progress Towards Effective Ocean Protection." *Marine Policy* 91: 11–13. doi:10.1016/j.marpol.2018.02.004.

Sánchez-Carnero, N., J. Ojeda-Zújar, D. Rodríguez-Pérez, and J. Márquez-Pérez. 2014. "Assessment of Different Models for Bathymetry Calculation Using SPOT Multispectral Images in a High-Turbidity Area: The Mouth of the Guadiana Estuary." *International Journal of Remote Sensing* 35 (2): 493–514. doi:10.1080/01431161.2013.871402.

Stumpf, R. P., K. Holderied, and M. Sinclair. 2003. "Determination of Water Depth with High-resolution Satellite Imagery over Variable Bottom Types." *Limnology and Oceanography* 48: 547–556. doi:10.4319/lo.2003.48.1_part_2.0547.

Su, H., H. Liu, and Q. Wu. 2015. "Prediction of Water Depth from Multispectral Satellite Imagery-The Regression Kriging Alternative." *IEEE Geoscience and Remote Sensing Letters* 12: 2511–2515. doi:10.1109/LGRS.2015.2489678.

Traganos, D., D. Poursanidis, B. Aggarwal, N. Chrysoulakis, and P. Reinartz. 2018. "Estimating Satellite-Derived Bathymetry (SDB) with the Google Earth Engine and Sentinel-2." *Remote Sensing* 10: 859. doi:10.3390/rs10060859.

Vahtmäe, E., and T. Kutser. 2016. "Airborne Mapping of Shallow Water Bathymetry in the Optically Complex Waters of the Baltic Sea." *Journal of Applied Remote Sensing* 10 (2): 025012. doi:10.1117/1.JRS.10.025012.

Wang, L., H. Liu, H. Su, and P. Wang. 2019. "Bathymetry Retrieval from Optical Images with Spatially Distributed Support Vector Machines." *GIScience & Remote Sensing* 56 (3): 323–337. doi:10.1080/15481603.2018.1538620.

Wölf, A. C., H. Snaith, S. Amirebrehimi, C. W. Devey, B. Dorschel, V. Ferrini, V. A. I. Huvenne, et al. 2019. "Seafloor Mapping – The Challenge of a Truly Global Ocean Bathymetry." *Frontiers in Marine Science* 6: 283. doi:10.3389/fmars.2019.00283.